Global return maps for mixed-mode oscillations with one fast and two slow variables

Christian Kuehn*

October 11, 2010

Abstract

Alternating patterns of small and large amplitude oscillations occur in a wide variety of physical, chemical, biological and engineering systems. These mixed-mode oscillations (MMOs) are often found in systems with multiple time scales. Previous differential equation modeling and analysis of MMOs has mainly focused on local mechanisms to explain the small oscillations. The goal of this paper is to provide a systematic starting point for the study of global return maps that generate the large oscillations. This paper contributes to the understanding of global return maps in the following ways: (a) We provide a detailed numerical study of the singular return maps for the Koper model which is a prototypical example for MMOs that also relates to local normal form theory, (b) we decompose the global return map to provide first steps towards towards analytical proofs of complicated MMO patterns, (c) we develop affine and quadratic return map models based on the previous analysis and (d) we demonstrate how to combine the global map models with small oscillations generated by two types of local normal forms. We find that the local-global decomposition is an efficient way to model, simulate and analyze MMOs.

Keywords: Fast-slow system, Koper model, return map, mixed-mode oscillations

1 Introduction

Mixed-mode oscillations (MMOs) are patterns of small and large amplitude oscillations in a time series that differ at least by one order in magnitude. They have been observed experimentally in the Belousov-Zhabotinsky reaction in the 1970's and 1980's [26, 35] and have been encountered more recently in a wide variety of different experiments [24, 25, 36, 11]. The basic classification has been based on counting the number of small s and large oscillations L so that we can symbolically represent an MMO by

$$\dots L_{j-1}^{s_{j-1}} L_j^{s_j} L_{j+1}^{s_{j+1}} \dots$$

*Max Planck Institute for the Physics of Complex Systems

where $j \in \mathbb{N}$ is an index. For example, if we have a periodic time series that has 2 large amplitude oscillations (LAOs) and then 3 small amplitude oscillations (SAOs) we get $\ldots 2^3 2^3 2^3 \ldots$ or simply an MMO of type 2^3. Systems exhibiting MMOs are often modeled using differential equations [6, 2]. Local bifurcation theory and numerical methods have been developed to gain a lot of insights into the generating mechanisms for the small amplitude oscillations of an MMO. A multiple time scale structure of the system is a key component for many local mechanisms. A detailed survey of this theory and its applications to particular models has been completed recently [9]. Therefore we shall only introduce necessary background instead of giving a detailed survey. Although the framework we present is mostly developed for the prototypical Koper model it is applicable many different models for MMOs.

In Section 2 we introduce the basic background from multiple time scale systems with two scales, so-called fast-slow systems. In Section 3 we briefly discuss folded node singularities and singular Hopf bifurcations; these two local mechanisms will be used as local components for the simulations in Section 7. In Section 4 the Koper model is introduced and its basic properties are discussed. The first main part of the numerical simulations are contained in Section 5; the global singular return map for the Koper model is decomposed into several more tractable flow maps. In Section 6 the global aspects of MMOs in the Koper model are analyzed using the flow maps. In Section 7 we consider a local-global decomposition of the MMO generating mechanisms; to demonstrate the feasibility of this approach we combine a global return map model with the two local mechanisms from Section 3. The numerical simulations show that typical MMO sequences can be reproduced by our hybrid method. Furthermore, it is easy to generate chaotic MMOs using this approach. In Section 8 we also give an outlook how analytical existence proofs for complicated MMO patterns can be carried out; the decomposition of maps is not only designed to yield numerical results but also to facilitate analytical proofs. Several other open problems are also highlighted.

2 Fast-Slow Systems

A fast-slow system of ordinary differential equations (ODEs) is given by:

$$\begin{array}{rcccl} \epsilon \dot{x} & = & \epsilon \frac{dx}{d\tau} & = & f(x,y), \\ \dot{y} & = & \frac{dy}{d\tau} & = & g(x,y), \end{array} \tag{1}$$

where $(x,y) \in \mathbb{R}^m \times \mathbb{R}^n$ and $\epsilon > 0$ is a small parameter representing the ratio of time scales. The maps f, g are assumed to be sufficiently smooth. The variables x are fast and the variables y are slow. We can change in (1) from the slow time scale τ to the fast time scale $t = \tau/\epsilon$ which yields

$$\begin{array}{rcl} x' & = & \frac{dx}{dt} = f(x,y), \\ y' & = & \frac{dy}{dt} = \epsilon g(x,y). \end{array} \tag{2}$$

To analyze (1)-(2) we consider the singular limit $\epsilon \to 0$. From equation (2) we obtain

$$\begin{array}{rcl} x' & = & f(x,y), \\ y' & = & 0, \end{array} \tag{3}$$

which is system of ODEs parameterized by the slow variables y. We call (3) the fast subsystem. The limit $\epsilon \to 0$ in (1) yields

$$\begin{aligned} 0 &= f(x,y), \\ \dot{y} &= g(x,y). \end{aligned} \tag{4}$$

System (4) is a differential-algebraic equation (DAE) called the slow subsystem. The flow induced by the slow (fast) subsystem is called the slow (fast) flow; continuous concatenations of fast and slow flow trajectories are called candidates or candidate orbits. Our main goal is to use the fast and slow subsystems to understand the dynamics of the full system (1)-(2) for $\epsilon > 0$. The algebraic constraint of (4) defines the critical manifold

$$C := \{(x,y) \in \mathbb{R}^m \times \mathbb{R}^n | f(x,y) = 0\}.$$

The points in C are equilibrium points for the fast subsystem (3). A subset $S \subset C$ is called normally hyperbolic if the $m \times m$ total derivative matrix $(D_x f)(p)$ is hyperbolic i.e. all eigenvalues have non-zero real parts for $p \in S$. We call a normally hyperbolic subset S attracting if all eigenvalues of $(D_x f)(p)$ have negative real parts for $p \in S$; similarly S is called repelling if all eigenvalues have positive real parts. On normally hyperbolic parts of C we can apply the implicit function theorem to $f(x,y) = 0$ providing a map $h(y) = x$ so that C can be expressed (locally) as a graph. Hence the slow subsystem (4) can be written as

$$\dot{y} = g(h(y), y). \tag{5}$$

To relate the dynamics of the slow flow to the dynamics of the full system for $\epsilon > 0$ the next theorem is of fundamental importance.

Theorem 2.1 (Fenichel's Theorem [13, 28, 9])**.** *Suppose $S = S_0$ is a compact normally hyperbolic submanifold of the critical manifold C. Then for $\epsilon > 0$ sufficiently small there exists a locally invariant slow manifold S_ϵ diffeomorphic to S_0. S_ϵ has a distance $O(\epsilon)$ from S_0 and the flow on S_ϵ converges to the slow flow as $\epsilon \to 0$. The slow manifold S_ϵ acquires the same stability properties of S_0 w.r.t. the fast variables.*

In general, slow manifolds are not unique but lie at $O(e^{-K/\epsilon})$-distance from each other for some $0 < K = O(1)$; due to this exponential closeness we often refer to "the" slow manifold. A trajectory of a general fast-slow system is called a canard if it is $O(\epsilon)$-close to a repelling slow manifold for a time that is $O(1)$ on the slow time scale [39]. A trajectory is called a maximal canard if it lies in the intersection of an attracting and a repelling slow manifold; note that this definition requires that we extend slow manifolds obtained by Fenichel's Theorem under the flow of the differential equation. For further references on fast-slow systems see [28, 29, 9, 1].

3 Two Local Mechanisms

Normal hyperbolicity can fail in several ways on subsets of the critical manifold C. The simplest case occurs when $(D_x f)(p)$ has a simple zero eigenvalue. We define a non-degenerate fold point $p \in C$ by requiring that

$$f(p) = 0, \qquad (D_x f)(p) \text{ has rank } m-1 \text{ with left and right null vectors } w \text{ and } v$$

and that C is locally parabolic near p

$$w \cdot [(D_{xx}f)(p)(v,v)] \neq 0 \qquad \text{and} \qquad w \cdot [(D_y f)(p)] \neq 0.$$

The set of fold points forms a manifold of codimension one in the m-dimensional critical manifold C. If $m = 1$ and $n = 2$ the fold points generically form a smooth curve that separates attracting and repelling sheets of the two-dimensional critical manifold C. We are going to restrict ourselves to the 3-dimensional case with $m = 1$ and $n = 2$ from now on. Two standard generating mechanisms for small oscillations will be considered in a normal form setup. Brøns, Krupa and Wechselberger [5] consider

$$\begin{aligned} \epsilon\dot{x} &= y - x^2, \\ \dot{y} &= -(\mu+1)x - z, \\ \dot{z} &= \tfrac{\mu}{2}, \end{aligned} \tag{6}$$

where x is the fast variable, (y, z) are the slow variables and μ is a parameter. The critical manifold for (6) is $C = \{y = x^2\}$ with a line of fold points $F = \{x = 0, y = 0\}$. The line F decomposes the critical manifold

$$C = C^r \cup F \cup C^a$$

where $C^r = C \cap \{x < 0\}$ is repelling and $C^a = C \cap \{x > 0\}$ is attracting. To derive the slow flow we can differentiate $y = x^2$ implicitly with respect to τ which gives $\dot{y} = 2x\dot{x}$. Therefore the slow flow is

$$\begin{aligned} \dot{x} &= \tfrac{-(\mu+1)x-z}{2x}, \\ \dot{z} &= \tfrac{\mu}{2}. \end{aligned} \tag{7}$$

Rescaling time by $\tau \mapsto 2x\tau$ reverses the direction of the flow on C^r and yields the desingularized slow flow

$$\begin{pmatrix} \dot{x} \\ \dot{z} \end{pmatrix} = \underbrace{\begin{pmatrix} -(\mu+1) & -1 \\ \mu & 0 \end{pmatrix}}_{=:A_0} \begin{pmatrix} x \\ z \end{pmatrix} \tag{8}$$

The desingularized slow flow has an equilibrium point at the origin $0 = (0, 0)$ contained in the fold line F; we say that 0 is a folded singularity/equilibrium of the slow flow. The eigenvalues $(\lambda_s, \lambda_w) = (-1, -\mu)$ of A_0 determine the type of the equilibrium; for $\mu < 0$ it is folded saddle, for $\mu > 0$ a folded node and for $\mu = 0$ a folded saddle-node of type II [39, 9]. We restrict ourselves to the folded node case and $\mu \in (0, 1)$ here. Then λ_s is associated to the strong eigendirection $\gamma_{s,0}$ and λ_w is associated to the weak eigendirection $\gamma_{w,0}$. Figure 1 sketches the flows (7)-(8) near 0. We refer to the extension of $\gamma_{s,0}$ ($\gamma_{w,0}$) under the slow flow as strong (weak) singular canard. Figure 1(a) shows a sector that is bounded by $\gamma_{s,0}$ and F. Trajectories in this sector can pass through from the attracting sheet C^a to the repelling sheet C^r; see Figure 1(b). We refer to this sector on C^a as the funnel region, or simply the funnel.

Folded nodes have been analyzed in detail. We briefly list the key results in a non-technical way.

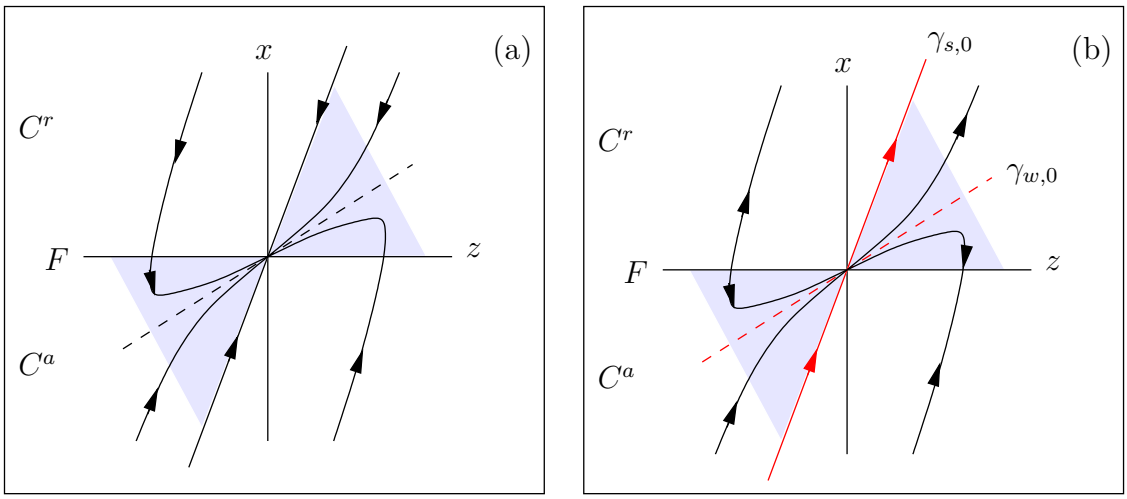

Figure 1: (a) The desingularized slow flow (8) is sketched for some $\mu > 0$ with a stable node at the origin. (b) The slow flow (7) is illustrated. The strong eigendirection (solid red) defines the strong singular canard $\gamma_{s,0}$; the weak eigendirection (dashed red) defines the weak singular canard $\gamma_{r,0}$.

- The singular canards $\gamma_{0,s}$ and $\gamma_{0,w}$ perturb to maximal canards $\gamma_{\epsilon,s}$ and $\gamma_{\epsilon,w}$ that lie in the intersection of the two slow manifolds $C^a_\epsilon \cap C^r_\epsilon$ [39].
- If $1/\mu \notin \mathbb{N}$ then there are further maximal canards arising as intersections of $C^a_\epsilon \cap C^r_\epsilon$, called secondary canards [41]. In particular, the attracting and repelling invariant manifolds twist around each other [18, 16].
- The number of twists of a trajectory in the fold region can be predicted using its distance δ relative to the strong singular canard and by the value of μ [5]. We agree to the convention that $\delta > 0$ indicates a trajectory entering the funnel region, $\delta = 0$ describes the strong canard and for $\delta < 0$ we are outside of the funnel.

Note carefully that the normal form (6) has no global equilibrium point for $\mu \in (0, 1)$. However, in many applications a Hopf bifurcation occurs near the onset of MMOs which suggests to consider the possibility of a global equilibrium point passing through the folded node region. Guckenheimer [17] suggested the following normal form for a singular Hopf bifurcation

$$\begin{aligned} \epsilon \dot{x} &= y - x^2, \\ \dot{y} &= z - x, \\ \dot{z} &= -\nu - ax - by - cz, \end{aligned} \tag{9}$$

where x is the fast variable, (y, z) are the slow variables and (ν, a, b, c) are parameters. The key difference between (6) and (9) is that we can find global equilibria for (9). They are determined by solving the equation

$$-\nu = (a + c)x + bx^2. \tag{10}$$

In particular if $\nu \approx 0$ then the equilibrium point is close to the folded singularity at the origin. The desingularized slow flow of (9) can be calculated similar to the folded node case

$$\begin{aligned} \dot{x} &= x - z \\ \dot{z} &= -2x(\nu + ax + bx^2 + cz) \end{aligned} \tag{11}$$

Note that a global equilibrium $q = q(\nu, a, b, c)$ determined by (10) is also an equilibrium for the slow flow. It can be shown [9, 34] that q is only important for the local dynamics near $(0, 0, 0)$ if ν is smaller than $O(\epsilon^{1/2})$. The key difference between MMOs that pass near a global equilibrium is that the SAOs can also be influenced by the stable and unstable manifolds $W^s(q)$ and $W^u(q)$. Detailed visualizations of the situation can be found in [9, 10]. Currently there is no complete unfolding available for the singular Hopf bifurcation (9); for partial results see [17] and for a detailed numerical study see [20]. Our main focus are the LAOs for an MMO and therefore we shall not provide further details on folded nodes and singular Hopf bifurcation. Instead we are going to use the normal forms (6) and (9) as "black-box" units for numerical simulation in Section 7.

4 The Koper Model

A typical model for MMOs is given by

$$\begin{aligned} \epsilon_1 \dot{x} &= y - x^3 + 3x, \\ \dot{y} &= kx - 2(y + \lambda) + z, \\ \dot{z} &= \epsilon_2(\lambda + y - z), \end{aligned} \tag{12}$$

where (k, λ) are the main bifurcation parameters and (ϵ_1, ϵ_2) are the singular perturbation parameters. The equations were first studied as a two-dimensional model by Boissonade and De Kepper [3] modeling a prototypical chemical reaction. Koper [31] added a third variable to a planar system and used numerical continuation techniques [15, 12] to study MMOs [31]. It is important to note that equations similar or equivalent to (12) have been proposed many times [14, 38, 30, 5, 32] as a "canonical" model for MMOs. The general idea to consider a cubic-shaped return mechanism can be traced back to van der Pol [7, 8]. The version (12) of Koper's model was proposed by the author and co-workers in [9]; it is obtained by a coordinate transformation of Koper's model and has the symmetry

$$(x, y, z, \lambda, k) \mapsto (-x, -y - z, -\lambda, k)$$

which allows us to restrict to parameter regions with $\lambda \geq 0$ or $\lambda \leq 0$ without loss of generality. If $0 < \epsilon_{1,2} \ll 1$ holds then (12) is a three time-scale system. We shall focus on the case $\epsilon_2 = 1$ and $0 < \epsilon_1 =: \epsilon \ll 1$ in which case we have one fast variable x and two slow variables (y, z). The critical manifold is

$$C_0 = \{(x, y, z) \in \mathbb{R}^3 : y = x^3 - 3x =: c(x)\}.$$

The typical cubic (or S-shaped) structure splits the critical manifold into three parts

$$C_0 = C^{a,-} \cup F_- \cup C^r \cup F_+ \cup C^{a,+}$$

where $C^{a,-} := C \cap \{x < -1\}$, $C^{a,+} := C \cap \{x > 1\}$ are normally hyperbolic attracting, $C^r := C \cap \{-1 < x < 1\}$ is normally hyperbolic repelling and

$$F_- := C \cap \{x = -1\} = \{(-1, 2, z)\} \qquad \text{and} \qquad F_+ := C \cap \{x = 1\} = \{(1, -2, z)\}$$

are fold curves curves of the critical manifold. MMOs can easily be observed in simulations; see Figure 2. The desingularized slow subsystem is

$$\begin{aligned} \dot{x} &= kx - 2(c(x) + \lambda) + z, \\ \dot{z} &= (3x^2 - 3)(\lambda + c(x) - z). \end{aligned} \tag{13}$$

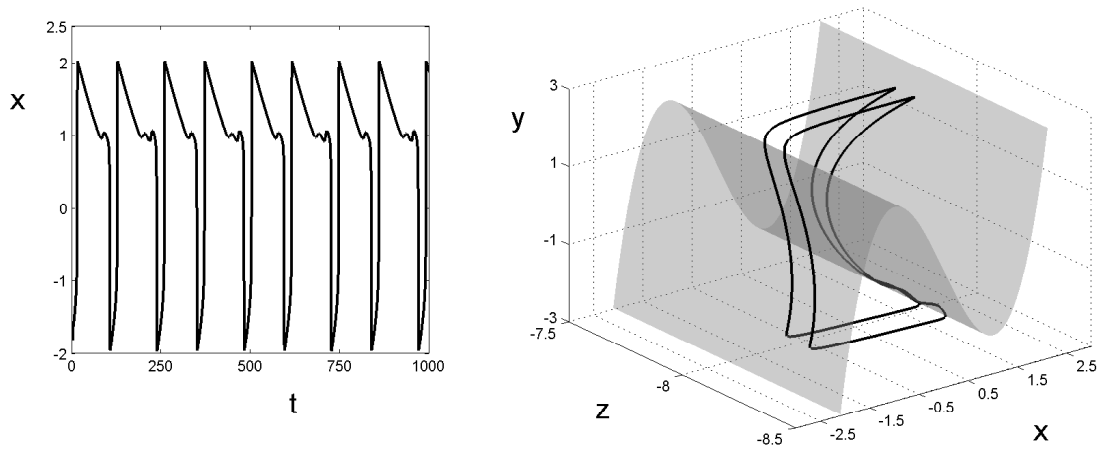

Figure 2: The parameter values for the simulation are $(\epsilon, k, \lambda) = (0.01, -10, -7)$. The time series for a $1^1 1^2$ MMO for the variable x is shown on the left and the phase space trajectory is shown on the right; the critical manifold C_0 is shown in grey.

There are two folded singularities

$$p_\pm = (\pm 1, 2\lambda \mp (4 + k)).$$

By symmetry we shall only focus on the folded singularity p_+. The linearization of the desingularized slow flow p_+ is

$$\begin{pmatrix} \dot{X} \\ \dot{Z} \end{pmatrix} = \begin{pmatrix} -10 & 1 \\ -6(8+\lambda) & 0 \end{pmatrix} \begin{pmatrix} X \\ Z \end{pmatrix} =: A_+ \begin{pmatrix} X \\ Z \end{pmatrix} \tag{14}$$

where we already set $k = -10$ which will fixed from now on. Note that in this case $\{X = 0\}$ corresponds to the fold line F_+ and p_+ is located at the origin. The eigenvalues of A_+ are

$$\sigma_w(\lambda) = -5 + \sqrt{-23 - 6\lambda} \qquad \text{and} \qquad \sigma_s(\lambda) = -5 - \sqrt{-23 - 6\lambda},$$

with associated eigenvectors

$$\Sigma_w(\lambda) = \begin{pmatrix} \frac{1}{5+\sqrt{-23-6\lambda}} \\ 1 \end{pmatrix} \qquad \text{and} \qquad \Sigma_s(\lambda) = \begin{pmatrix} \frac{1}{5-\sqrt{-23-6\lambda}} \\ 1 \end{pmatrix}.$$

Therefore p_+ is a folded saddle for $\lambda < -8$, a folded saddle-node of type II (FSN II [39, 9]) for $\lambda_{\text{FSN II}} = -8$ and a folded node for $\lambda \in (-8, -23/6)$. At $\lambda_{nf} = -23/6$ the transition from a folded node to a folded focus occurs. The singular Hopf bifurcation for the full system occurs $O(\epsilon)$ away from $\lambda_{\text{FSN II}}$. It is supercritical and the stable global equilibrium q loses stability at this point. Therefore the interesting parameter region for MMOs is

$$\lambda \in (\lambda_{\text{FSN II}}, \lambda_{nf}) = (-8, -23/6), \qquad k = -10.$$

Note that this parameter region represents a typical one-parameter MMO sequence [9]. The important eigenvector for global returns is Σ_s associated to the strong primary canard as it bounds the rotational sectors lying on $C^{a,+}$. The x-component Σ_s^x of Σ_s lies, for the scaling we have chosen, between $\Sigma_s^x(-8) = \infty$ and $\Sigma_s^x(-23/6) = \frac{1}{5}$. Therefore the rotational sectors [5] that subdivide the funnel region are given by a convex cone with opening angle between $\frac{\pi}{2}$ and $\cos^{-1}(25/26)$. This finishes a basic local analysis of the Koper model and we can start with the main part of our investigation in the next section.

5 Return map(s)

Our goal is to analyze the structure of the global singular return map. We fix $\epsilon = 0$ and recall that $k = -10$. Then we focus on λ as the primary bifurcation parameter. In this case the folded node p_+ and the unique equilibrium q account for the SAOs. Observe that global returns to a neighborhood of p_+ can be decomposed. See Figure 3 for an illustration of the one-dimensional singular maps we are going to define:

(a) Trajectories can reach the fold line F_+ at a jump point and follow the fast flow to the drop curve $L^{a,-} := C \cap \{x = -2\}$. Then trajectories follow the slow flow induced by (13) to F_- and jump to the drop curve $L^{a,+} := C \cap \{x = 2\}$. We denote this map by

$$m_j : F_+ \to L^{a,-} \to F_- \to L^{a,+}$$

where j indicates that we consider a regular jump. We denote the intermediate map by $m_{a-} : L^{a,-} \to F_-$. Observe that if we parameterize the domain and range by z then the intermediate map m_{a-} is the only non-trivial component of the map m_j and the other parts of m_j are the identity with respect to z.

(b) Trajectories can flow into the folded node p_+. Suppose we consider trajectories tracking the part of the strong canard γ_s contained in C^r. These trajectories jump at some point from γ_s to $C^{a,-}$ and flow into F_- before jumping to $L^{a,+}$. Denote this map by

$$m_f : \gamma_r \to C^{a,-} \to F_- \to L^{a,+}$$

where f indicates a jump forward (or away) singular canard orbit; again observe that only the part $C^{a,-} \to F_-$ is non-trivial with respect to z.

(c) Trajectories tracking the strong canard $\gamma_s \subset C^r$ can also jump at some point from γ_s to $C^{a,+}$ and flow into F_+. It will be advantageous to terminate this map at a line $L^\mu := C \cap \{x = 1 + \mu\}$ for some $\mu \geq 0$ sufficiently small. Then we have a map

$$m_b : \gamma_r \to C^{a,+} \to L^\mu$$

where b indicates a jump backwards (or back) singular canard orbit.

(d) There is also a map induced by the slow flow on $C^{a,+}$ starting from the drop curve $L^{a,+}$ towards the fold line

$$m_{a+} : L^{a,+} \to L^{\mu}$$

(e) The linearization (14) at the folded singularity p_+ can be used to define a flow map in the fold region

$$m_s : L^{\mu} \to F_+$$

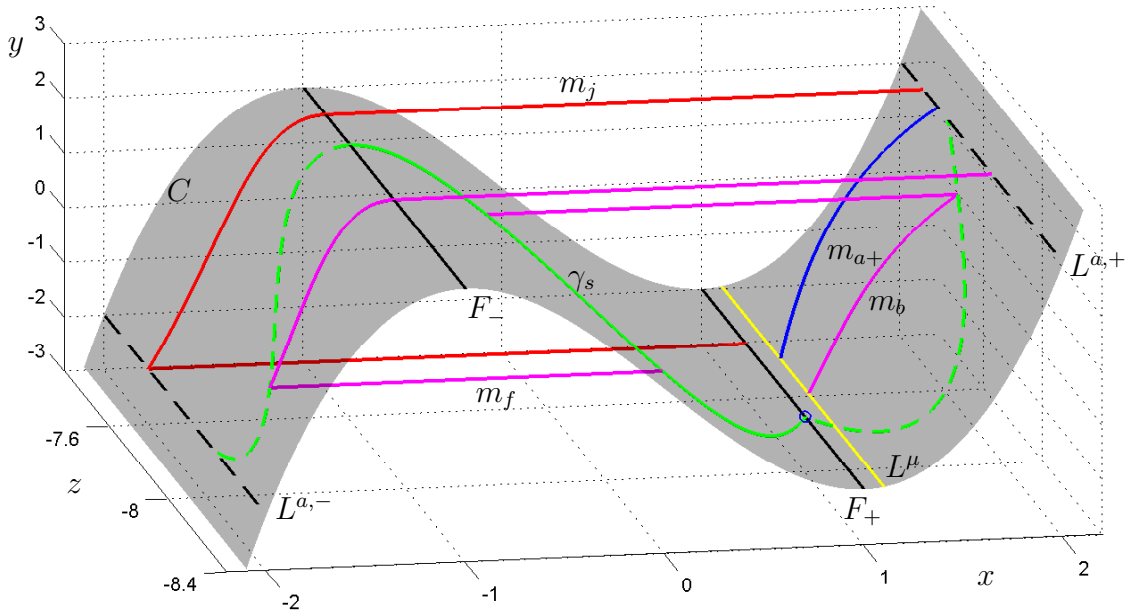

Figure 3: Illustration of the singular map decomposition; parameter values are $(\epsilon, k, \lambda) = (0, -10, -7)$. Definitions of all maps and domains are given at the beginning of Section 5. Here we show: the critical manifold C (grey), the strong canard $\gamma_s \subset C^m$ (green) and its projections to $C^{a,\pm}$ (dashed green), the fold lines $F_\pm$ (black) and their projections $L^{a,\mp}$ (dashed black, $\mu = 0.1$), the line L^{μ} (yellow) and the folded node p_+ (blue circle). Examples for the maps m_j (red, regular jump), m_{a+} (blue, flow towards F_+), m_f (magenta, jump forward canard) and m_b (magenta, jump backward canard) are displayed as well.

Figure 4 shows representatives of the maps m_j, m_{a+}, m_b and m_f for $\lambda = -7$ with respect to the variable z. The first observation is that the maps are surprisingly "regular". For example, m_j is essentially affine. The map $m_{a,+}$ can be well-approximated by a quadratic map, or even an affine map if we neglect the approach of the trajectories near the folded singularity that causes the nonlinearity. The maps induced from the projections of the strong canard $\gamma_s \subset C^r$ onto $C^{a,\pm}$ are multi-valued when parameterized with respect to z due to the fold structure of γ_s; see Figure 3. With another parameterization we expect that m_b and m_f are generically single-valued by uniqueness of solutions for the desingularized slow subsystem. The parameterization with respect to z is very convenient and we see from Figure

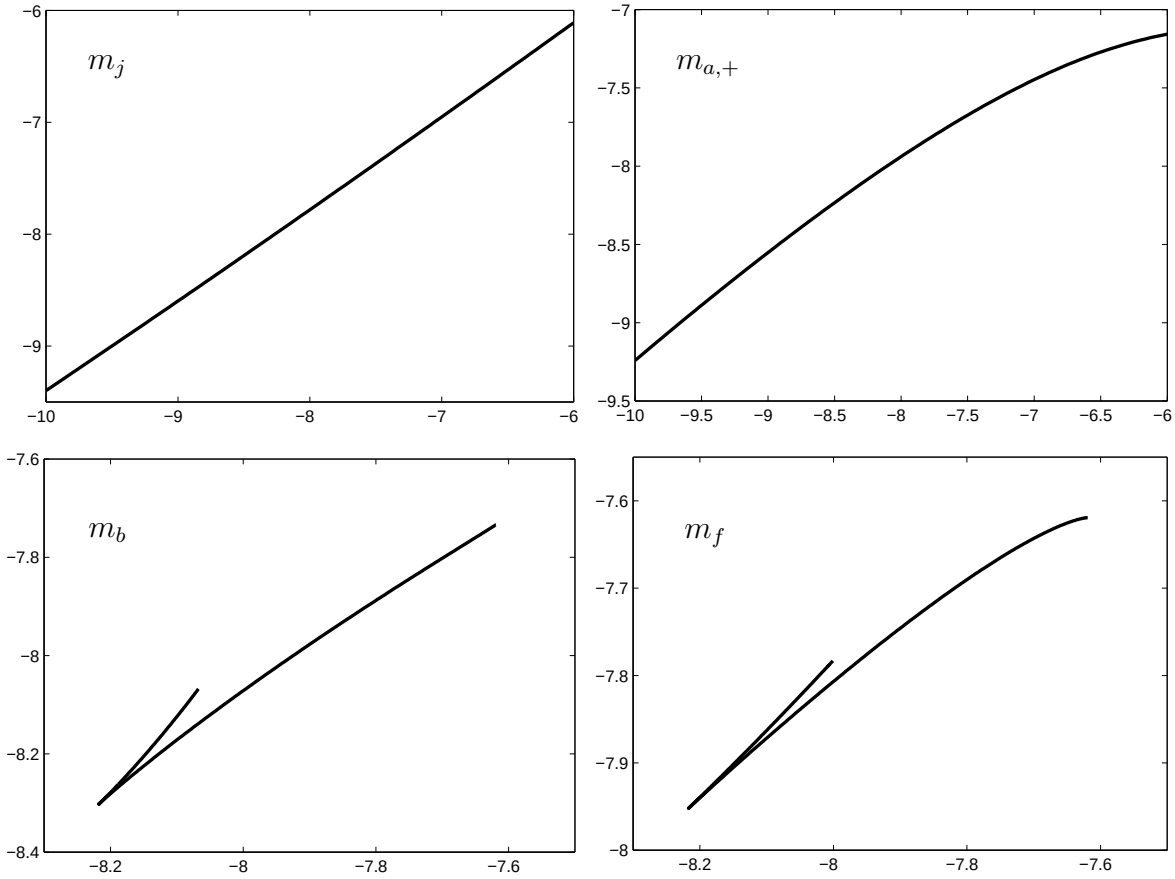

Figure 4: Singular maps with respect to the z-variable i.e. the horizontal axis shows $z = z_{in}$ and the vertical axis shows $z_{out} = m_K(z_{in})$ for $K \in \{j, (a,+), b, f\}$.

4 that the upper and lower branches of the map will be well approximated by affine and/or quadratic maps. Hence we make the following ansatz:

$$m_K(z) = c_2(\lambda)z^2 + c_1(\lambda)z + c_0(\lambda)$$

for each map m_K with $K \in \{j, (a,+), b, f\}$ where the coefficients $c_{0,1,2}(\lambda)$ are to be determined. We are going to illustrate the procedure for finding the coefficients for m_f and just state the results we obtained for the other three maps. The ansatz is that m_f can be decomposed as follows:

$$m_f(z) = \begin{cases} c_1^{fu}(\lambda)z + c_0^{fu}(\lambda) & \text{if } z_{min}^{fu}(\lambda) \le z \le z_{max}^{fu}(\lambda) \\ c_2^{fl}(\lambda)z^2 + c_1^{fl}(\lambda)z + c_0^{fl}(\lambda) & \text{if } z_{min}^{fl}(\lambda) \le z \le z_{max}^{fl}(\lambda) \\ \text{undefined} & \text{otherwise} \end{cases} \tag{15}$$

where we impose continuity at the shared boundary point $m_f(z_{min}^{fu}) = m_f(z_{min}^{fl})$. See Figure 5 for an example. In Figure 5 the upper part of m_f is approximated by an affine map and the lower part by a quadratic. Simulating $\lambda \in (\lambda_{\text{FSN II}}, \lambda_{nf})$ we observe that this type of approximation can be used throughout the parameter interval.

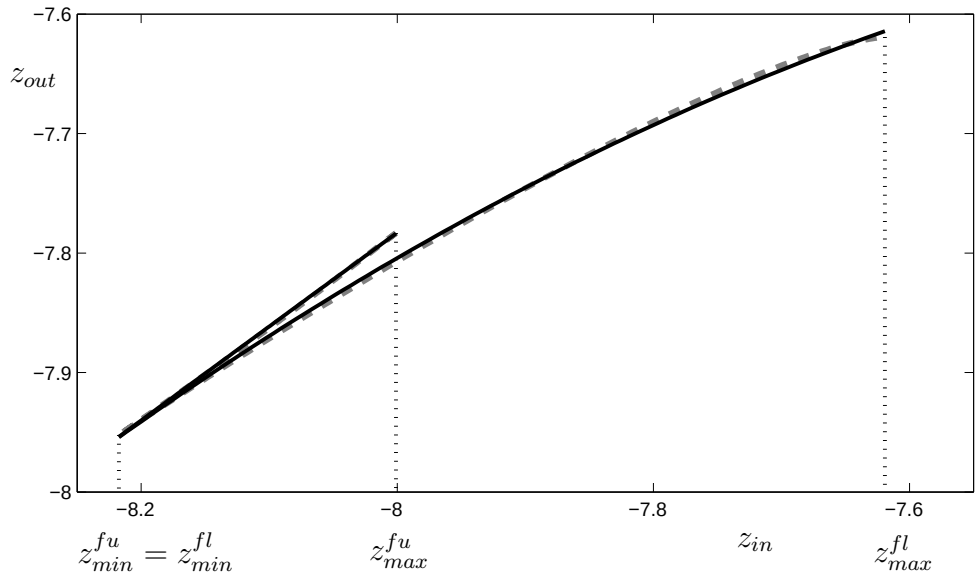

Figure 5: Singular map m_f with $z_{out} = m_f(z_{in})$. The computed map is shown as a dashed grey curve and the approximations are shown in solid black (affine for upper part and quadratic for lower part). The bounds of the domains for each part of the map are marked as well (dotted vertical lines).

As a next step we have to determine all functions depending on λ in (15). The boundary z_{max}^{fu} is given by the folded singularity p_+ so that $z_{max}^{fu}(\lambda) = 2\lambda + 6$. We also know from the definition of (15) that $z_{min}^{fu} = z_{min}^{fl}$. The other functions of λ can only be approximated numerically due to the nonlinear slow flows on C^r, which defines γ_s, and on $C^{a,-}$, which defines the map to F_-. Figure 6 shows numerical computations of the unknown functions of

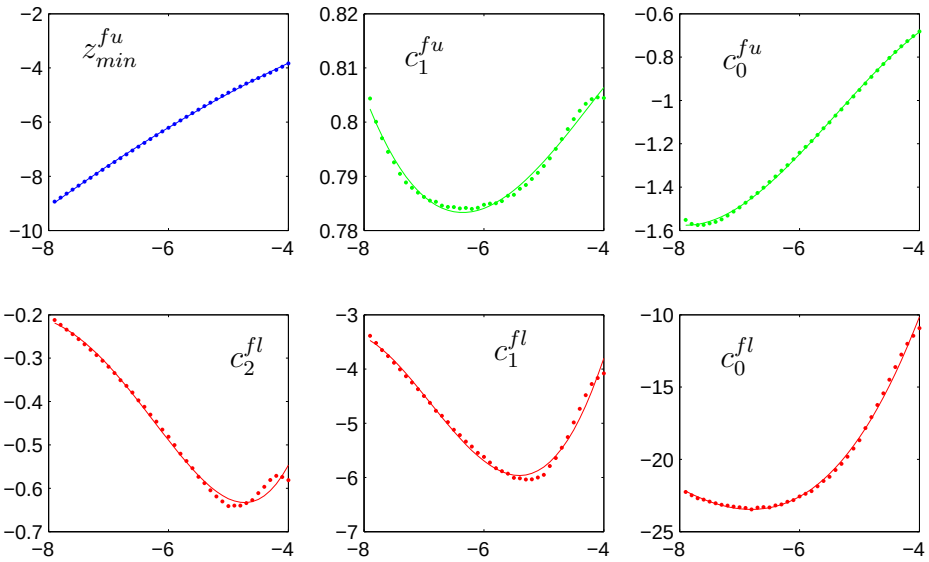

Figure 6: Horizontal axes are λ and vertical axes are the respective coefficients e.g. top left figure shows $z_{min}^{fu}(\lambda)$. The only relevant part for the definition of (15) that is not shown is z_{max}^{fl} which is as regular (almost linear) as the other parts of the domain boundaries for m_f. The dots are computed points and the curves provide polynomial fits (quadratic=blue, cubic=green and quartic=red).

λ in the definition of m_f in (15).

Several observations can be made from Figure 6 and the previous remarks. All the domain boundaries $z_{min}^{fu}(\lambda)$, $z_{max}^{fu}(\lambda)$, $z_{min}^{fl}(\lambda)$ and $z_{max}^{fl}(\lambda)$ are very regular and depend (almost) linearly on λ. The coefficients of the linear and quadratic polynomials have substantial nonlinear dependencies on λ for the entire range $\lambda \in (\lambda_{\text{FSN II}}, \lambda_{nf})$. This implies that although affine and quadratic maps can be very good approximants at fixed parameter values it will be more difficult to analyze the global return maps inducing MMOs as parameter-dependent families. For the other maps m_b, m_j and $m_{a,+}$ we propose the following approximations:

$$m_b(z) = \begin{cases} c_2^{bu}(\lambda)z^2 + c_1^{bu}(\lambda)z + c_0^{bu}(\lambda) & \text{if } z_{min}^{bu}(\lambda) \le z \le z_{max}^{bu}(\lambda) \\ c_1^{bl}(\lambda)z + c_0^{bl}(\lambda) & \text{if } z_{min}^{bl}(\lambda) \le z \le z_{max}^{bl}(\lambda) \\ \text{undefined} & \text{otherwise} \end{cases} \tag{16}$$

$$m_j(z) = c_1^j(\lambda)z + c_0^j(\lambda) \tag{17}$$

$$m_{a,+}(z) = c_2^a(\lambda)z^2 + c_1^a(\lambda)z + c_0^a(\lambda) \tag{18}$$

where we impose continuity at the shared boundary point for m_b i.e. $m_b(z_{min}^{bu}) = m_b(z_{min}^{bl})$. As a next step we are going to calculate the map for the linearized desingularized slow flow near p_+. The intersection of the eigendirection of Σ_s with $L^\mu = \{x = 1 + \mu\}$ is easily

calculated as

$$(1, 2\lambda + 6)^T + \left(\mu, \frac{\mu}{\Sigma_s^x(\lambda)}\right)^T = (1 + \mu, 2\lambda + 6 + \mu(5 - \sqrt{-23 - 6\lambda})) =: (1 + \mu, z^\mu(\lambda))$$

Hence all trajectories that arrive at L^μ with $z \geq z^\mu(\lambda)$ will stay in the funnel and reach p_+ while trajectories for $z < z^\mu(\lambda)$ will first reach the fold line F_- and jump to $L^{a,-}$. To see where on F_+ the last class of trajectories ends up we could just solve (14). Note however that there exists a very good approximation for $z < z^\mu(\lambda)$ that just amounts to projecting $(\mu, Z(0))$ parallel to Σ_s onto $\{X = 0\}$ which is given by

$$(\mu, Z(0)) \mapsto \left(0, Z(0) - \frac{\mu}{\Sigma_s^x}\right)$$

Therefore we get the local representation for the map m_s in (X, Z)-coordinates

$$m_s^{loc}(Z) = \begin{cases} 2\lambda + 6 & \text{if } z \geq z^\mu(\lambda) \\ 2\lambda + 6 + Z - \frac{\mu}{\Sigma_s^x} & \text{if } z < z^\mu(\lambda) \end{cases}$$

If z is the coordinate obtained in original coordinates without linearization then

$$m_s(z) = \begin{cases} 2\lambda + 6 & \text{if } z \geq z^\mu(\lambda) \\ z - \frac{\mu}{\Sigma_s^x} & \text{if } z < z^\mu(\lambda) \end{cases}$$

With the different maps available we can proceed to analyze how they can be used to explain the global returns that generate LAOs.

6 Mixed-Mode Oscillations

Remark: Throughout this section we work with the polynomial approximations to the maps $m_{(.)}$ that have been derived in the last section.

The first question we shall consider is what happens to trajectories that do not follow the canard $\gamma_s \subset C^r$ when arriving at p_+ or which land outside of the funnel region. The relevant map for this purpose is

$$(m_{a,+} \circ m_j) : F_+ \cap \{z \leq 2\lambda + 6\} \to L^\mu \tag{19}$$

We are interested when part of the domain of (19) is returned inside the funnel so that $(m_{a,+} \circ m_j)(z) > z^\mu(\lambda)$. Figure 7 shows the map (19) for three different values of λ. We observe that closer to the folded saddle-node of type II (i.e. near the singular Hopf bifurcation) trajectories that arrive outside the funnel on F_+ can get mapped back into the funnel under (19). For $\lambda = -6.5$ in Figure 7 we observe that no trajectories can return into the funnel and that the return map $(m_s \circ m_{a,+} \circ m_j)$ will have a stable fixed point since μ is small and hence the projection m_s will preserve the intersection with the diagonal.

Hence we can consider several quantitative questions:

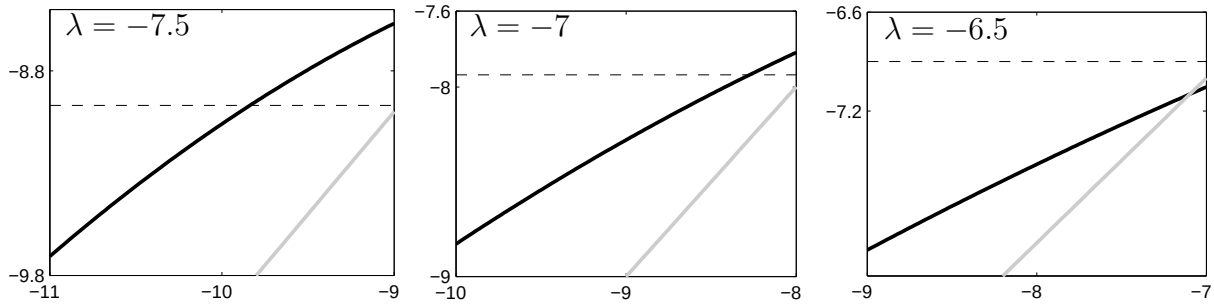

Figure 7: Map $(m_{a,+} \circ m_j)(z)$, approximated by (17) and (18) with $k = -10$ and $\mu = 0.1$. Horizontal axes are input z-coordinates on a domain $z \in ((2\lambda + 6) - 2, 2\lambda + 6) \subset F_+$ and vertical axes are $(m_{a,+} \circ m_j)(z)$ (think black curves). The location of the folded node funnel region $z^\mu(\lambda)$ is shown by horizontal dashed black lines and the diagonal is indicated by the thick grey line.

1. For what values of λ do trajectories from outside the funnel re-enter it?
2. When does the map $(m_s \circ m_{a,+} \circ m_j)$ have fixed points? When does the fixed point coincide with the folded node p_+?
3. How are trajectories mapped into the funnel? More precisely, what is the dependence of the distance δ to the strong singular canard $\gamma_s \cap C^{a,+}$ upon varying λ?

A trajectory starting for $z < 2\lambda + 6$ will re-enter the funnel after one global return if and only if

$$\begin{aligned}(m_{a,+} \circ m_j)(z) &= c_2^a(\lambda)(c_1^j(\lambda)z + c_0^j(\lambda))^2 + c_1^a(\lambda)(c_1^j(\lambda)z + c_0^j(\lambda)) + c_0^a(\lambda) \\ &= c_2^a(c_1^j)^2 z^2 + \left(2c_2^a c_1^j + c_1^a c_1^j\right) z + (c_0^j)^2 c_2^a + c_1^a c_0^j + c_0^a < z^\mu(\lambda)\end{aligned}$$

By monotonicity of (19) on the required interval (see Figure 7) we can just pick the folded node $z = 2\lambda + 6$ and determine when the condition fails; this yields the critical parameter value at which not all trajectories near p_+ return to the funnel in one iteration. We find that the parameter value at which p_+ gets returned to the boundary of the funnel is $\lambda = \lambda_r \approx -6.7887$. Next, we consider the fixed points of $(m_s \circ m_{a,+} \circ m_j)$. Those points correspond to candidates representing relaxation oscillations. We find that at $\lambda = \lambda_r$ a stable fixed point appears for the map $(m_s \circ m_{a,+} \circ m_j)$. Therefore we conjecture that a transition to relaxation oscillations occurs near λ_r for the full system and ϵ sufficiently small; this can be confirmed by numerical continuation [9]. Note that the bifurcation that creates the fixed point occurs at the boundary of the domain of $(m_s \circ m_{a,+} \circ m_j)$.

As a next step we consider candidates that follow the canard $\gamma_s \cap C^r$ i.e. we consider the maps m_f and m_b. We start with m_b which represents medium-size canard-induced oscillations if trajectories from the domain of m_b re-enter the funnel after one iteration step. Figure 8 plots three examples of the map m_b. The closer the parameter values are to the folded saddle-node of type II at $\lambda = -8$ the larger is the part of $\gamma_s \cap C^r$ that returns inside the funnel. The closer we are to relaxation oscillation at $\lambda = \lambda_r$ the more of $\gamma_s \cap C^r$ gets

mapped outside the funnel.

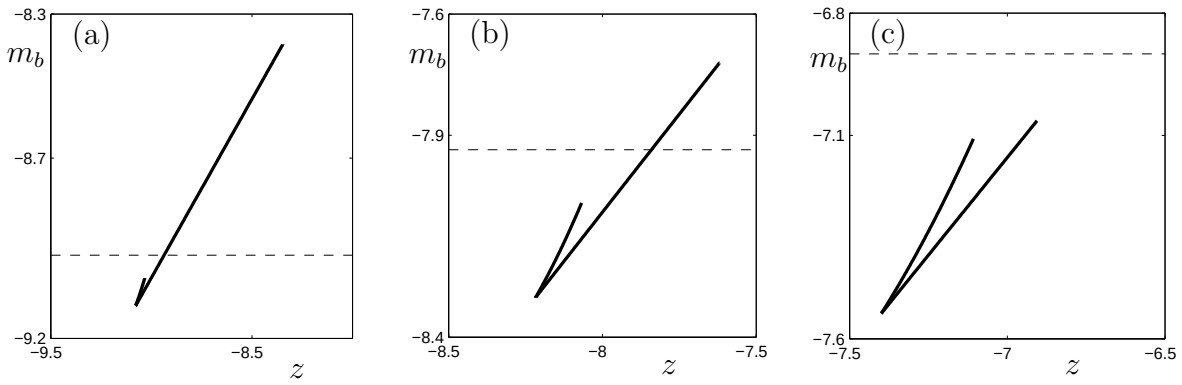

Figure 8: Singular maps with respect to the z-variable i.e. the horizontal axis shows $z = z_{in}$ and the vertical axis shows $m_b = m_b(z_{in})$. The horizontal dashed line indicates the funnel boundary $z^\mu(\lambda)$; here $\mu = 0.1$. (a) $\lambda = -7.5$, (b) $\lambda = -7$ and (c) $\lambda = -6.5$.

Note that near $\lambda = -8$ with $\lambda > -8$ we must always have some part of $\gamma_s \cap C^r$ near p_+ that does get mapped outside the funnel since the opening cone angle of the funnel region is less than $\frac{\pi}{2}$; see Section 4. Therefore there is always one part inside and one part outside the funnel for jump back canard orbits. Orbits in the full system that follow γ_s^ϵ for an $O(1)$-time on the slow time scale and get mapped back to $C^{a,+}$ via perturbation of m_b represent intermediate oscillations.

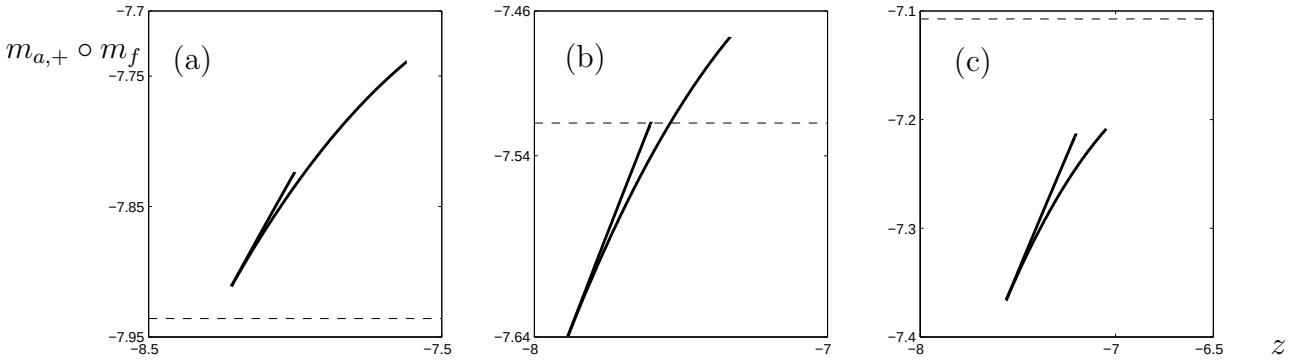

Figure 9: Singular maps with respect to the z-variable i.e. the horizontal axis shows $z = z_{in}$ and the vertical axis shows $m_{a,+} \circ m_f = (m_{a,+} \circ m_f)(z_{in})$. The horizontal dashed line indicates the funnel boundary $z^\mu(\lambda)$; here $\mu = 0.1$. (a) $\lambda = -7$, (b) $\lambda = -6.8$ and (c) $\lambda = -6.6$.

For the map m_f we immediately consider $m_{a,+} \circ m_f$ to see how jump forward canards get returned relative to the funnel. Figure 9 shows that there is a very rapid transition from jump forward canards that end all in the funnel for $\lambda = -7$ (Figure 9(a)), a splitting

of jump forward canards with respect to the funnel (Figure 9(b)) and all jump forward canards outside the funnel for $\lambda = -6.6$ (see Figure 9(c)). Let us consider the case when the entire jump forward canards end up in the funnel. This can be interpreted as a global MMO generating mechanism via canards. More precisely, a trajectory of the full system can make small oscillations near a folded node, follow $C^r \cap \gamma_s$ closely producing an intermediate oscillation and then return into the funnel. This provides a mechanism to transition small loops into large ones via canards. The closer we get to $\lambda = \lambda_r$ the more excursions outside the funnel occur which means that in this region we expect more mixed behavior of MMOs of type L^s with $L > 1$. Since the resonances $1/\mu \in \mathbb{N}$ for the eigenvalues [41] of the folded node are fewer near λ_r we also expect s to decrease if we increase λ. Hence we conjecture that MMO sequences near a singular Hopf bifurcation will produce patterns with $s \gg 1$ and small L while away from the singular Hopf L^s patterns with $L \sim s$ are more likely to occur.

7 A Local-Global Model

We have seen that the global singular return maps for the Koper model are very regular and can often be described as affine or quadratic maps. The only feature of the global returns that is complicated to describe are canard orbits that follow the strong canard $\gamma_s \cap C^r$. These orbits describe intermediate oscillations i.e. orbits that, under parameter variation will grow to a large relaxation loop or decay to a small oscillation. We do not consider these intermediate orbits for now. We propose the following local/global description of MMOs near a folded node respectively a folded-saddle node. We assume without loss of generality that the folded singularity is located at the origin $(x, y, z) = (0, 0, 0)$. For the local dynamics we use the normal forms (6) and (9). Recall that the critical manifold of both normal forms is

$$C_0 = \{(x, y, z) \in \mathbb{R}^3 : y = x^2\}$$

It is attracting for $x > 0$ and repelling for $x < 0$ and we denote the two branches of C_0 by C_0^a and C_0^r. The associated attracting slow manifold provided by Fenichel Theory is

$$C_\epsilon^a = \{(x, y, z) \in \mathbb{R}^3 : x = h_\epsilon^a(y, z)\}$$

where the map h_ϵ^a is given by the implicit function theorem and $h_0^a(y, z) = \sqrt{y}$. Define two sections

$$\begin{aligned} \Sigma_1 &:= \{(x, y, z) \in \mathbb{R}^3 | x = k_1\} \\ \Sigma_2 &:= \{(x, y, z) \in \mathbb{R}^3 | x = -k_2\} \end{aligned}$$

for suitable fixed $k_j > 0$, $k_j = O(\sqrt{\epsilon})$ with $j = 1, 2$. The choice of scaling $O(\sqrt{\epsilon})$ is prescribed by the fact that outside of a neighborhood of size $O(\sqrt{\epsilon})$ of the origin Fenichel Theory applies. Define a map

$$m_{12} : \Sigma_1 \to \Sigma_2$$

by the flow map of (6) or (9). Note that the sections Σ_j are naturally parameterized by the coordinates (y, z). The global return map $m_{21} : \Sigma_2 \to \Sigma_1$ will be modeled as follows:

$$\begin{aligned} m_{21}(y,z) &= \begin{pmatrix} k_1^2 \\ m(z) \end{pmatrix} + \epsilon \left[\begin{pmatrix} a_{11} & a_{12} \\ a_{21} & a_{22} \end{pmatrix} \begin{pmatrix} y \\ z \end{pmatrix} + \begin{pmatrix} b_1 \\ b_2 \end{pmatrix} \right] + O(\epsilon^2) \\ &= (k_1^2, m(z))^T + \epsilon[A(y,z)^T + b] + O(\epsilon^2) \end{aligned} \tag{20}$$

where $m(z) = m_2 z^2 + m_1 z + m_0$ and we require that the matrix A is invertible. Note that we can make several further choices e.g. we could decide to include higher-order terms or to assume that $m(z)$ is modeled as an affine map and set $m_2 = 0$. Note that the map m_{21} has to satisfy a further constraint if we assume that all trajectories approach the origin exponentially close to the slow manifold C_ϵ^a; this requires

$$k_2\sqrt{\epsilon} = (h_\epsilon^a \circ m_{21})(y, z)$$

Another constraint to generate MMOs is that the global map m_{21} maps some part of its domain close to the perturbation of the folded node funnel region. Although the model (20) has formally nine free parameters m_i, a_{jk}, b_l we can view m_{21} as an $O(\epsilon)$-perturbation of the leading order term which has only two or three parameters depending on the choice of model ($m_2 = 0$ or $m_2 \neq 0$). Hence the description is low-dimensional, explicit and de-couples the local and global bifurcation structure of the problem. To illustrate the effect of global bifurcation parameters we numerically investigate two typical bifurcation sequences, one for each local normal form with fixed local parameters. The numerical simulations are going to show that the hybrid approach to MMOs is very successful numerically and can re-produce all the main sequences obtained in applications.

Remark: In the following, we are going to visualize the LAOs in a time series for the hybrid system defined by m_{12} and m_{21} by inserting a large amplitude oscillation at fixed amplitude whenever the map m_{21} is applied.

For the folded node (6) we fix the parameters $(\epsilon, \mu) = (0.01, 0.006)$. Since $2k + 1 < \frac{1}{\mu} < 2k + 3$ for $k = 82$ we know from folded node theory that there will be $k + 2 = 84$ canards [5, 9]. The theory also predicts that the maximum number of small oscillations is $k + 1$. In Figure 10 we varied the global return mechanism to demonstrate that we can systematically reach sectors near a folded node with a sub-maximal number of oscillations and different MMO signatures. The global return map is chosen as the lowest order approximating linear map with $m(z) = 0.1z + m_0$ and $A = 0$, $b = 0$. The parameter m_0 is viewed as the main bifurcation parameter and controls the entry of trajectories to the different folded node rotation sectors. We find the following MMO signatures:

$m_0 =$	-0.015	-0.01	-0.005	-0.0025	-0.001	0.0
$L^s =$	1^{14}	1^9	1^4	1^2	2^1	1^0

Maximal MMO signatures can also be obtained but many of the small oscillations will be at an exponentially small scale due to the contraction towards the weak canard [9]. Observe

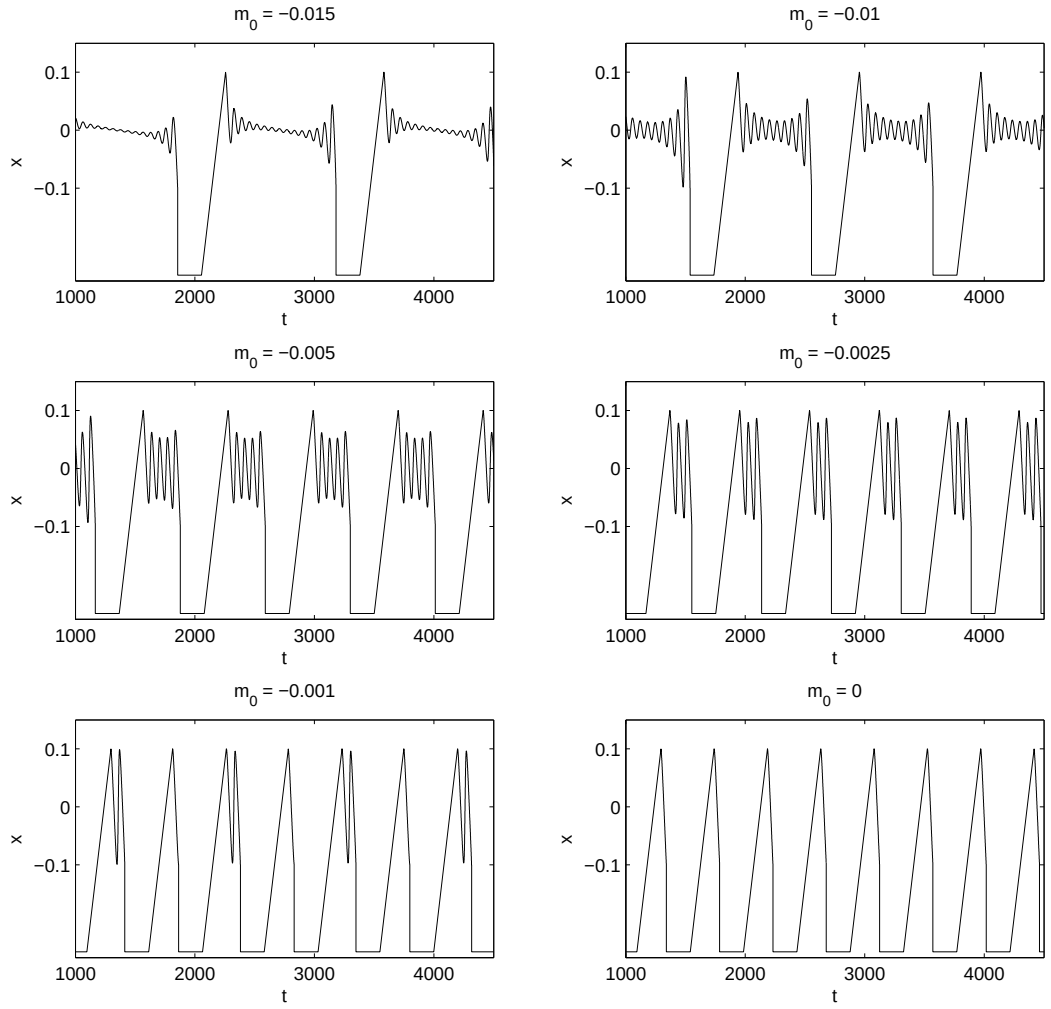

Figure 10: MMOs generated by the hybrid system with local dynamics (6) (parameters $\epsilon = 0.01$ and $\mu = 0.006$) and global dynamics $m(z) = 0.1z + m_0$ with $k_1 = \sqrt{\epsilon}$. The hybrid transition from local to global dynamics has been applied when $x < -\sqrt{\epsilon}$. Trajectories have been started at $(x, y, z) = (\sqrt{\epsilon}, \epsilon, 0.15)$.

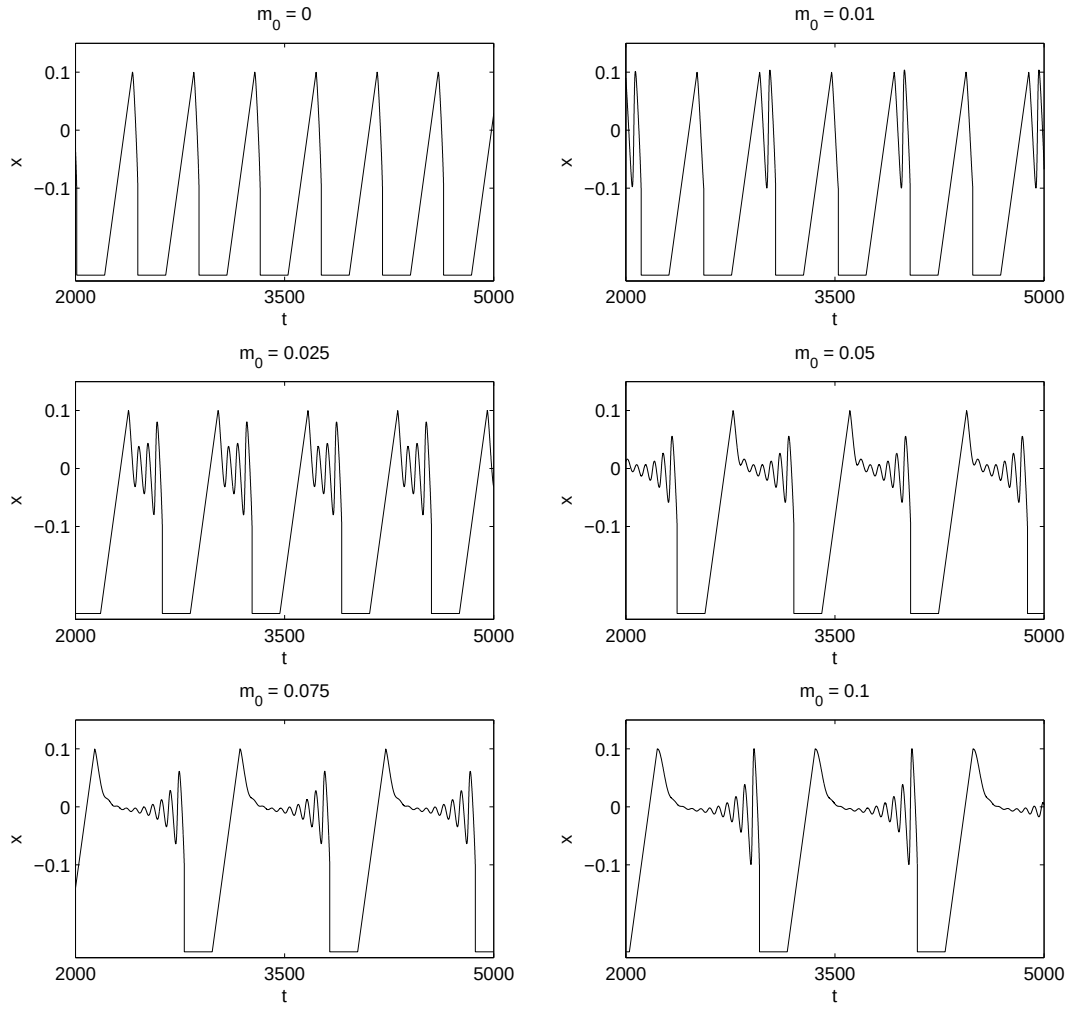

Figure 11: MMOs generated by the hybrid system with local dynamics (9) (parameters $(\epsilon, \nu, a, b, c) = (0.01, 0.015, 0.5, -1, 1)$) and global dynamics $m(z) = 0.1z + m_0$ with $k_1 = \sqrt{\epsilon}$. The hybrid transition from local to global dynamics has been applied when $x < -\sqrt{\epsilon}$. Trajectories have been started at $(x, y, z) = (\sqrt{\epsilon}, \epsilon, 0.15)$.

that we have efficiently un-coupled the local dynamics from the global dynamics. This shows what role the local and global dynamics play in the generation of an L^s-signature.

The second simulation focuses on the singular Hopf normal form (9). We fix the parameters $(\epsilon, \nu, a, b, c) = (0.01, 0.01, 0.5, -1, 1)$. For the global return map we again consider the singular limit of m_{21} with parameter $m_2 = 0$, $m_1 = 0.1$ and primary bifurcation parameter m_0. It is easy to check that the equilibrium near the fold curve is located at $q = (x_{eq}, y_{eq}, z_{eq}) \approx (-6.63729 \times 10^{-3}, 4.40537 \times 10^{-5}, -6.63729 \times 10^{-3})$. The equilibrium is a saddle-focus with one-dimensional stable and two-dimensional unstable manifold. We are in the regime where the SAOs are generated/amplified via the singular Hopf mechanism. Figure 11 shows the typical SAOs with increasing amplitude as they approach $W^u(q)$. We find the following MMO signatures:

$m_0 =$	0.0	0.01	0.025	0.05	0.075	0.1
$L^s =$	1^0	2^1	1^3	1^6	1^9	1^9

It is important to note that the number of SAOs for the singular Hopf bifurcation is not only influenced by the folded node but also by the relative positions of the invariant manifolds of q. In particular, Guckenheimer [17] points out that the one-dimensional stable manifold $W^s(q)$ seems to interact in an intricate way with MMO trajectories. Our method of hybrid simulation is well-suited to investigate this dependency further once the local unfolding of the singular Hopf bifurcation is better understood [20]. Also for the singular Hopf bifurcation we have been able to re-produce a typical MMO sequence without varying the local parameters. Extensive additional numerical simulation showed that it is difficult to produce periodic sequences of MMOs of the forms

$$L^s, \quad \text{with } L \gg 1, s \gg 1 \qquad \text{and} \qquad L_1^{s_1} L_2^{s_2} \cdots \tag{21}$$

by varying further parameters in the map $m(z)$. These simulations confirm parts of the incomplete theory for MMOs in three dimensions [32, 33] which predict the limited number of MMO patterns for three time scale systems. It has been conjectured in [9] that higher-dimensional return maps will be needed to find more complicated MMOs of the form (21).

Chaotic MMO signatures can be produced easily using a suitable quadratic map with $m_2 \neq 0$. Figures 12 and 13 illustrate an orbit obtained from the hybrid system of the singular Hopf bifurcation with global returns generated by the map $m(z) = 3z^2 + 0.2z - 0.8$; the irregular behaviour of the global returns in Figure 12 suggests that this orbit is chaotic. It is well-known that systems with two slow variables and one fast variable with S-shaped critical manifold can be chaotic [23, 21]. Koper [31] observed chaotic regions in parameter space in his original analysis of (12); transitions of MMOs to chaotic sequences can also be observed in many other models [9]. As shown above, our hybrid model is also able to reproduces this aspect of typical MMO models.

From the numerical simulations in this section we conclude that the hybrid modeling approach can be very useful to investigate the dependence of MMOs on parameters. It allows to reproduce the main dynamical features and to de-couple the global from the local dynamics.

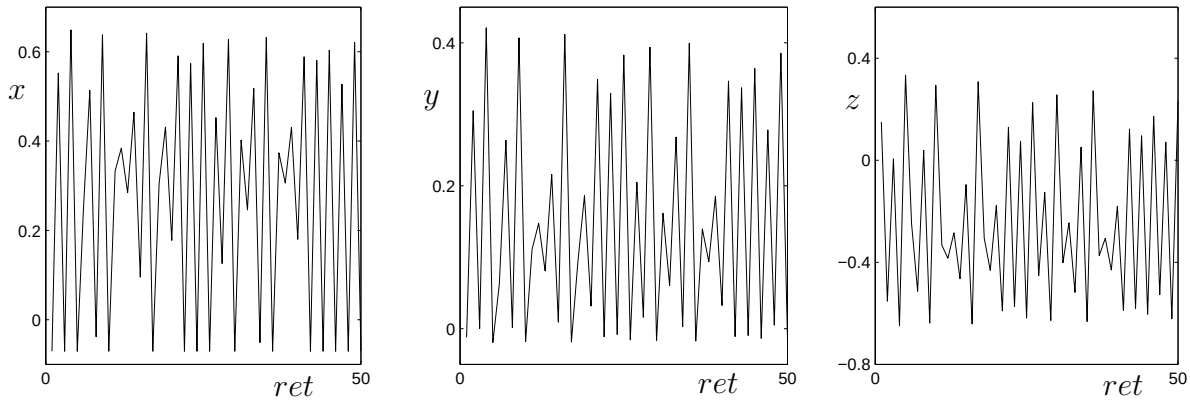

Figure 12: Coordinates (x, y, z) before the global map is applied; the entire orbits are generated by the hybrid system with local dynamics (9) (parameters $(\epsilon, \nu, a, b, c) = (0.01, 0.015, 0.5, -1, 1)$) and global dynamics $m(z) = 3z^2 + 0.2z - 0.8m_0$ with $k_1 = \sqrt{\epsilon}$. The hybrid transition from local to global dynamics has been applied when $x < -\sqrt{\epsilon}$. The times series of the returns shows typical chaotic non-periodic behaviour.

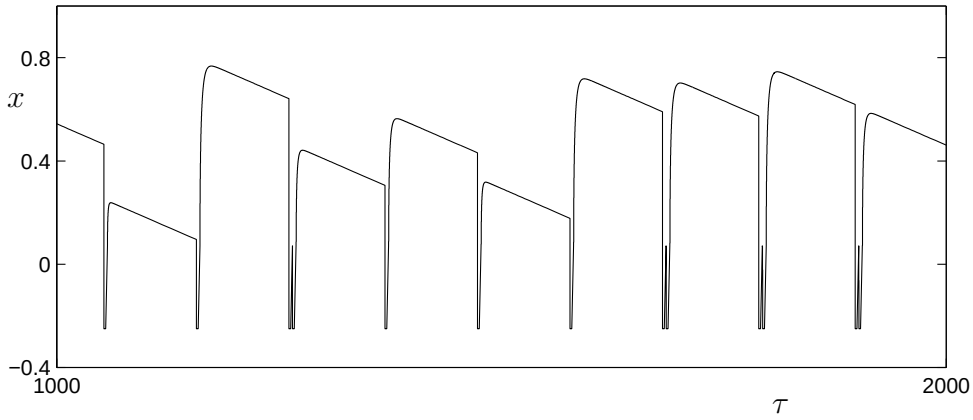

Figure 13: Subset of the time series in (x, τ) variables associated to the returns in Figure 12. Irregular oscillations are observed with 1^0 and 1^1 components.

8 Discussion

Observe that both our local-global models we have discussed in the previous section can be used to facilitate rigorous existence proofs of L^s patterns using the following steps:

(P1) Decompose the system into a local mechanism generating the SAOs and a global mechanism generating the LAOs.

(P2) Use the unfolding of the local mechanism to describe a flow map. This map can be used to prove the existence of s small oscillations. For folded nodes the required theory is available while for singular Hopf the local theory is under active development.

(P3) Decompose the global return map, as described in Section 5 for the Koper model, into fast and slow parts. For each part of the flow, the fast and slow subsystems provide the zeroth-order approximation. Use results about transitions at singularities (e.g. at regular folds, [40]) or the exchange lemma [27] to couple the different parts of the global flow map.

(P4) This procedure provides an analytic description of the local-global hybrid system used in this section for numerical simulation.

Unfortunately it is often very difficult to prove the required estimates in (P3). This can be seen in the Koper model for the map m_{a-} that is given by the slow flow on an attracting critical manifold. Indeed, we would have to estimate the flow for a general 2-dimensional nonlinear ODE which is a non-trivial task. Often interval arithmetic is used in this context [22]. The numerical computation of bifurcations for decomposed maps can often be carried out [19, 4] which implies that we can at least compute a conjecture before the start of the proof. To avoid these complications another strategy is to assume the form of the global return map (e.g. a one-dimensional quadratic map or a two-dimensional diffeomorphism). In this approach the global maps should be viewed as one- or two-dimensional families to study the generic global returns and their bifurcations. A successful example of this method in a different context is the analysis of homoclinic bifurcations [37].

Other open questions that we have not addressed in this paper are the following:

- A detailed bifurcation analysis of a hybrid model with quadratic return map would be desirable to gain better insight what influence each parameter of the global map $m(z) = m_2z^2+m_1z+m_0$ has on the dynamics. This should also allow us to understand in more detail how large regions of different types of MMOs are in parameter space.

- Another interesting study would be to consider two-parameter bifurcation diagrams that vary one local parameter of the normal form and one global parameter of the return.

- It would also be desirable to investigate a prototypical model for MMOs that has two fast and two slow variables using our approach of decomposing global return maps.

We leave these three projects to future work. We expect them to be particularly fruitful once more details about the singular Hopf unfolding are known.

References

[1] V.I. Arnold. *Encyclopedia of Mathematical Sciences: Dynamical Systems V*. Springer, 1994.

[2] D. Barkley. Slow manifolds and mixed-mode oscillations in the Belousov-Zhabotinskii reaction. *J. Chem. Phys.*, 89(9):5547–5559, 1988.

[3] J. Boissonade and P. DeKepper. Transitions from bistability to limit cycle oscillations. Theoretical analysis and experimental evidence in an open chemical system. *J. Phys. Chem.*, 84:501–506, 1980.

[4] K. Bold, C. Edwards, J. Guckenheimer, S. Guharay, K. Hoffman, J. Hubbard, R. Oliva, and W. Weckesser. The forced van der pol equation 2: Canards in the reduced system. *SIAM Journal of Applied Dynamical Systems*, 2(4):570–608, 2003.

[5] M. Brøns, M. Krupa, and M. Wechselberger. Mixed mode oscillations due to the generalized canard phenomenon. *Fields Institute Communications*, 49:39–63, 2006.

[6] H. Degn, L.F. Olsen, and J.W. Perram. Bistability, oscillation, and chaos in an enzyme reaction. *Annals of the New York Academy of Sciences*, 316(1):623–637, 1979.

[7] B. Van der Pol. On relaxation oscillations. *Philosophical Magazine*, 7:978–992, 1926.

[8] B. Van der Pol. The nonlinear theory of electric oscillations. *Proc. IRE*, 22:1051–1086, 1934.

[9] M. Desroches, J. Guckenheimer, C. Kuehn, B. Krauskopf, H. Osinga, and M. Wechselberger. Mixed-mode oscillations with multiple time scales. *submitted*, 2010. http://www.mpipks-dresden.mpg.de/∼ckuehn/PDF_files/mmo_survey_preprint.pdf.

[10] M. Desroches, B. Krauskopf, and H.M. Osinga. Mixed-mode oscillations and slow manifolds in the self-coupled FitzHugh-Nagumo system. *Chaos*, 18, 2008.

[11] C.T. Dickson, J. Magistretti, M.H. Shalisnky, B. Hamam, and A. Alonso. Oscillatory activity in entorhinal neurons and circuits: Mechanisms and function. *Ann. N.Y. Acad. Sci.*, 911:127–150, 2006.

[12] E.J. Doedel, A. Champneys, F. Dercole, T. Fairgrieve, Y. Kuznetsov, B. Oldeman, R. Paffenroth, B. Sandstede, X. Wang, and C. Zhang. Auto 2007p: Continuation and bifurcation software for ordinary differential equations (with homcont). *http://cmvl.cs.concordia.ca/auto*, 2007.

[13] N. Fenichel. Geometric singular perturbation theory for ordinary differential equations. *Journal of Differential Equations*, 31:53–98, 1979.

[14] A. Goryachev, P. Strizhak, and R. Kapral. Slow manifold structure and the emergence of mixed-mode oscillations. *J. Chem. Phys.*, 107(18):2881–2889, 1997.

[15] W.F. Govaerts. *Numerical Methods for Bifurcations of Dynamical Equilibria*. SIAM, 1987.

[16] J. Guckenheimer. Return maps of folded nodes and folded saddle-nodes. *Chaos*, 18, 2008.

[17] J. Guckenheimer. Singular Hopf bifurcation in systems with two slow variables. *SIAM J. Appl. Dyn. Syst.*, 7(4):1355–1377, 2008.

[18] J. Guckenheimer and R. Haiduc. Canards at folded notes. *Mosc. Math. J.*, 5(1):91–103, 2005.

[19] J. Guckenheimer, K. Hoffman, and W. Weckesser. The forced van der Pol equation 1: The slow flow and its bifurcations. *SIAM Journal of Applied Dynamical Systems*, 2(1):1–35, 2003.

[20] J. Guckenheimer and P. Meerkamp. Bifurcation analysis of singular hopf bifurcation in $\mathbb{R}^3$. *in preparation*, 2010.

[21] J. Guckenheimer, M. Wechselberger, and L.-S. Young. Chaotic attractors of relaxation oscillations. *Nonlinearity*, 19:701–720, 2006.

[22] R. Haiduc. Horseshoes in the forced van der pol equation. *PhD Thesis - Cornell University*, 2005.

[23] R. Haiduc. Horseshoes in the forced van der Pol system. *Nonlinearity*, 22:213–237, 2009.

[24] T. Hauck and F.W. Schneider. Mixed-mode and quasiperiodic oscillations in the peroxidase-oxidase reaction. *J. Phys. Chem.*, 97:391–397, 1993.

[25] M.J.B. Hauser and L.F. Olsen. Mixed-mode oscillations and homoclinic chaos in an enzyme reaction. *J. Chem. Soc. Faraday Trans.*, 92(16):2857–2863, 1996.

[26] J.L. Hudson, M. Hart, and D. Marinko. An experimental study of multiple peak periodic and nonperiodic oscillations in the belousov-zhabotinskii reaction. *J. Chem. Phys.*, 71(4):1601–1606, 1979.

[27] C. Jones and N. Kopell. Tracking invariant manifolds with differential forms in singularly perturbed systems. *Journal of Differential Equations*, pages 64–88, 1994.

[28] C.K.R.T. Jones. *Geometric Singular Perturbation Theory: in Dynamical Systems (Montecatini Terme, 1994)*. Springer, 1995.

[29] T.J. Kaper and C.K.R.T. Jones. A primer on the exchange lemma for fast-slow systems. *in: Multiple-Time-Scale Dynamical Systems*, IMA Vol. 122:65–88, 2001.

[30] A.L. Kawczynski and P.E. Strizhak. Period adding and broken Farey tree sequences of bifurcations for mixed-mode oscillations and chaos in the simplest three-variable nonlinear system. *J. of Chem. Phys.*, 112(14):6122–6130, 2000.

[31] M.T.M. Koper. Bifurcations of mixed-mode oscillations in a three-variable autonomous Van der Pol-Duffing model with a cross-shaped phase diagram. *Physica D*, 80:72–94, 1995.

[32] M. Krupa, N. Popovic, and N. Kopell. Mixed-mode oscillations in three time-scale systems: A prototypical example. *SIAM J. Applied Dynamical Systems*, 7(2), 2008.

[33] M. Krupa, N. Popovic, N. Kopell, and H.G. Rotstein. Mixed-mode oscillations in a three time-scale model for the dopaminergic neuron. *Chaos*, 18, 2008.

[34] M. Krupa and M. Wechselberger. Local analysis near a folded saddle-node singularity. *preprint*, 2009.

[35] J. Maselko and H.L. Swinney. Complex periodic oscillation and Farey arithmetic in the Belousov-Zhabotinskii reaction. *J. Chem. Phys.*, 85:6430–6441, 1986.

[36] M. Orban and I.R. Epstein. Chemical oscillators in group VIA: The Cu(II)-catalyzed reaction between hydrogen peroxide and thiosulfate ion. *J. Am. Chem. Soc.*, 109:101–106, 1987.

[37] L.P. Shilnikov. A case of the existence of a denumerable set of periodic motions. *Sov. Math. Dokl.*, 6:163–166, 1965.

[38] P.E. Strizhak and A.L. Kawczynski. Regularities in complex transient oscillations in the belousov-zhabotinsky reaction in a batch reactor. *J. Phys. Chem.*, 99:10830–10833, 1995.

[39] P. Szmolyan and M. Wechselberger. Canards in $\mathbb{R}^3$. *Journal of Differential Equations*, 177:419–453, 2001.

[40] P. Szmolyan and M. Wechselberger. Relaxation oscillations in $\mathbb{R}^3$. *Journal of Differential Equations*, 200:69–104, 2004.

[41] M. Wechselberger. Existence and bifurcation of canards in $\mathbb{R}^3$ in the case of a folded node. *SIAM J. Applied Dynamical Systems*, 4(1):101–139, 2005.